

Beyond lock-in analysis for volumetric imaging in apertureless scanning near-field optical microscopy

R. VOGELGESANG, R. ESTEBAN & K. KERN
Max Planck Institut für Festkörperforschung, 70569 Stuttgart, Germany

Key words. apertureless SNOM, mechanical anharmonicity, volumetric imaging.

Summary

Conventional apertureless scanning near-field optical microscopy uses lock-in demodulation techniques to filter higher harmonics from the periodically modulated optical signal. On the one hand, this signal notoriously may contain contaminating mechanical contributions; on the other, it reduces the available data to one number per pixel. Realizing that the vertically oscillating near-field probe actually traverses a whole *volume* above the sample surface, we discuss a model to extend the data analysis in an attempt to better extract the optical information and to recover its three-dimensional spatial distribution.

Introduction

Scanning near-field optical microscopy (SNOM) is a powerful technique that overcomes the spatial resolution limit of conventional far-field lens or mirror objectives by utilizing near-field optical interactions (Synge, 1928; Okeefe, 1956; Ash & Nicholls, 1972; Pohl *et al.*, 1984; Lewis *et al.*, 1984; Betzig *et al.*, 1991). The scattering type or apertureless SNOM (aSNOM) is a popular example of SNOM implementations based on dynamic mode atomic force microscopes (AFMs). It has been demonstrated to offer local field mapping (Zenhausern *et al.*, 1994, 1995; Martin *et al.*, 1996; Hillenbrand & Keilmann 2000) and material contrast (Knoll & Keilmann 1999, 2000; Ocelic & Hillenbrand 2004). It has also been used to obtain Raman and fluorescence information (Hartschuh *et al.*, 2003; Hu *et al.*, 2003; Gerton *et al.*, 2004; Huang *et al.*, 2005). In this kind of instrument, optical radiation excites highly localized near fields in the spatial region between the tip apex and the sample surface resulting in scattered radiation that carries optical information with a

spatial resolution given essentially by the effective radius of curvature of the tip apex.

For the extraction of such information, the AFM is operated in non-contact mode, i.e. the tip-sample distance d is modulated. The instantaneous dependence of the scattered optical field on this distance leads to a corresponding current signal $\mathcal{I}(d)$ generated in the photodetector used to collect the scattered radiation. A periodic mechanical oscillation $d(t)$ of the tip-sample distance with angular frequency Ω induces a periodic modulation of the optical interaction in the tip-sample system. All harmonics $k\Omega$, ($k = 0, 1, 2, \dots$) of the temporal current signal $\mathcal{I}(d(t))$ carry information, which is in general a non-trivial combination of optical (nonlinear $\mathcal{I}(d)$) and mechanical (anharmonic $d(t)$) influences (Bek *et al.*, 2005).

We note that lock-in filtering at one of the harmonics of Ω reduces the time traces of the optical signal from each pixel to a single complex-valued number. It essentially projects the 3D information from the volume encompassed by the oscillating AFM tip into a flat surface. An alternative analysis technique capable of providing the scattered fields for each location in this volume was recently presented by (Diziain *et al.*, 2006). It considers a negligible anharmonicity in the cantilever oscillation, a frequent assumption in aSNOM, which requires great care in the choice of scanning conditions. Generally, though, the cantilever motion $d(t)$ is always more or less anharmonic. Intrinsically, this is because of the anharmonic potentials describing the *mechanical* bending of the cantilever carrying the tip and the non-linear tip-sample forces (Hillenbrand *et al.*, 2000; Stark *et al.*, 2000; Lee *et al.*, 2002, 2003; Garcia & Perez, 2002; Stark & Heckl, 2003; Rodriguez & Garcia 2004; Stark, 2004). Extrinsically, the AFM feedback control, which is used to ensure a constant height of the oscillating tip above the sample surface, may also introduce anharmonicity. These contributions emerge in the higher harmonics of the temporal current signal $\mathcal{I}(d(t))$ predominantly by a combination with the relatively strong linear background to $\mathcal{I}(d)$.

Correspondance to: Dr. Ralf Vogelgesang, Tel +49(0)7116891581; E-mail: r.vogelgesang@fkf.mpg.de; homepage:www.fkf.mpg.de/kern

A general connection of the local optical fields and their localized interaction with the scanning tip apex has long been appreciated. However, idealized assumptions about this relation are typically not verified. For example, signals measured at the k th harmonic of the AFM frequency are not in general given by k th spatial derivatives but depend even qualitatively on the chosen tip oscillation amplitude (Barchiesi & Groszes, 2005). A deeper look into possibilities of reconstructing the optical nearfields is very much necessary – also to facilitate comparison with realistic numerical simulations (Esteban *et al.*, 2007). Here we present a model that allows obtaining 3D aSNOM information and which includes the presence of anharmonicities in the cantilever motion. Its possibilities and limitations to decouple the mechanical and optical components are discussed.

Analytical framework

In Bek *et al.* (2005), we introduced a model that allows to analyze the competing influences on the contrast formation in aSNOM. At heart, it represents a nested expansion of the spatial dependence of the optical signal and the cantilever oscillation. With the goal in mind that a given measured data set should be analyzed efficiently, the choice of expansions is such that only a few significant terms contribute to the description of a realistic scenario. When evaluated algebraically, the resulting model function is a complex series that is less than ideal for a general purpose of numerical fitting to measured data. Especially, a change in the choice of model parameters used is cumbersome to facilitate. For this purpose, it is better to keep the truncated nested expansion in its implicit form. Here, we demonstrate a straightforward procedure to use this expansion with efficient numerical optimization algorithms such as the Levenberg–Marquardt algorithm (Press *et al.*, 1992).

We choose a complex-valued version for the Fourier expansion in harmonics of the fundamental oscillation frequency for the oscillation of the cantilever position,

$$d(t) = \sum_{k=-N_k}^{N_k} d_k \exp(ik\Omega t) \quad (1)$$

because of the conceptual ease of interpretation of the measured values obtained from a dual-phase lock-in measurement. Here $\Omega = 2\pi/T$ is the (angular) oscillation frequency of the cantilever, N_k is the highest overtone modelled and d_k is the amplitude of the k th overtone. Note that the requirement $d_{-k} = \overline{d_k}$ for a real-valued $d(t)$ implies that they can be described by $2N_k + 1$ free real-valued parameters. These are the average location d_0 and modulus and phase of all harmonics included. A purely harmonic mechanical motion is described by $N_k = 1$, whereas anharmonic contributions are included if we set $N_k > 1$.

For the dependence of the photocurrent on the tip-sample distance we use the Taylor expansion

$$\mathcal{I}(d) = \sum_{m=0}^{N_m} \frac{1}{m!} (d - d_r)^m \mathcal{I}^{(m)}, \quad (2)$$

where N_m is the highest number Taylor expansion coefficient included. A purely linear optical signal is described by $N_m = 1$. With $N_m > 1$ we include contributions to the instantaneous optical signal, which vary nonlinearly with the tip location. $\mathcal{I}^{(m)}$ is the m th derivative of the photocurrent with respect to tip-sample distance at a distance d_r , typically chosen at some point of the tip trajectory to minimize the error after truncation of the series (Bek *et al.*, 2005). It is convenient to absorb this parameter of the Taylor expansion in the zeroth Fourier coefficient by renaming $(d_0 - d_r \rightarrow d_0)$ or equivalently identifying the reference point of the scale with zero $d_r = 0$. This is assumed throughout this paper. We obtain a model function $\mathcal{I}(d(t))$, which we can use to analyze a set of measured data.

Lock-in demodulation

For simplicity, we consider a time series of N photocurrent values \mathcal{I}_j , measured at regular intervals $t_j = j\Delta t$. Oftentimes, one chooses to feed these data to the signal input of a dual-phase lock-in amplifier, with a reference signal at the n th harmonic frequency. Assuming the measurements are taken sufficiently frequently ($\Delta t \ll T$) and in sufficient number ($N\Delta t \gg T$), we can express the lock-in filtered value by

$$\mathcal{S}_n = \frac{1}{N\Delta t} \sum_j \mathcal{I}_j \exp(-in\Omega t_j) \Delta t. \quad (3)$$

Note that from the whole time series of measured data a *single* complex-valued number is extracted, representing an amplitude and a phase. This value we compare with a corresponding idealized model measurement,

$$\begin{aligned} \mathcal{S}_n &= \frac{1}{T} \int_t \mathcal{I}(d(t)) \exp(-in\Omega t) dt \quad (4) \\ &= \mathcal{I}^{(0)} \delta_{0n} \\ &\quad + \mathcal{I}^{(1)} \sum_{\kappa_1=n} d_{\kappa_1} \\ &\quad + \frac{1}{2} \mathcal{I}^{(2)} \sum_{\kappa_1+\kappa_2=n} d_{\kappa_1} d_{\kappa_2} \\ &\quad + \frac{1}{6} \mathcal{I}^{(3)} \sum_{\kappa_1+\kappa_2+\kappa_3=n} d_{\kappa_1} d_{\kappa_2} d_{\kappa_3} \\ &\quad + \dots, \quad (5) \end{aligned}$$

where the different κ_j can take both positive and negative integer values. Apparently, \mathcal{S}_n is a complicated mixture of mechanical and optical contributions. Even for purely harmonic cantilever motion ($d(t) = d_{-1} \exp(-i\Omega t) + d_0 +$

$d_1 \exp(i\Omega t)$) the resulting expression does not simplify much,

$$S_n = \sum_{m=n}^{\infty} \frac{1}{m!} \mathcal{I}^{(m)} \sum_{q=0}^{(m-n)/2} \binom{m}{m-n-2q} d_0^{m-n-2q} \times \binom{n+2q}{n+q} d_1^{n+q} d_{-1}^q. \quad (6)$$

In the particular relevant case of a cantilever oscillation just above the sample surface, we choose the reference point $d_r = 0$ at the surface. Writing $d_1 = |d_1| \exp(i\phi_1)$, we find in this case $|d_1| = |d_{-1}| = d_0/2$ and $d(t) = 2|d_1| [1 + \cos(\Omega t + \phi_1)]$. Under these conditions,

$$S_n = \exp(in\phi_1) \sum_{m=n}^{\infty} \frac{1}{m!} \mathcal{I}^{(m)} |d_1|^m \sum_{q=0}^{(m-n)/2} 2^{m-n-2q} \times \binom{m}{m-n-2q} \binom{n+2q}{n+q}. \quad (7)$$

This is the signal measured by conventional lock-in amplifier filtering of the aSNOM signal – assuming perfectly harmonic cantilever motion. Only if we consider infinitesimal oscillation amplitudes $2|d_1|$ we find that

$$S_n = \frac{\exp(in\phi_1)}{n!} \mathcal{I}^{(n)} |d_1|^n \quad (8)$$

is essentially given by the n th derivative of the optical signal along the direction of the motion of the cantilever. As the oscillation amplitude is increased towards realistic values, however, higher order terms become non-negligible and Eq. (7) is not quite straightforward to interpret. In principle the different $\mathcal{I}^{(m)}$ values could be determined from a series of measurements using different oscillation amplitudes $2|d_1|$, ultimately leading to a complete reconstruction of the signal versus distance curve $\mathcal{I}(d)$. Experimentally, though, this is a cumbersome approach and it is interesting to explore options of using the acquired N data points in other ways than the relatively simple lock-in filtering.

Least squares modelling

If we can disentangle the mechanical and optical contributions to $\mathcal{I}(t)$ using our model, we can extract more than just the single number S_n for each sample surface location. It should be possible to obtain the spatial dependence $\mathcal{I}(d)$ for the *whole* trajectory of the tip in space, i.e. at each pixel, we obtain a vertical line of data.

We consider a fitting procedure that determines values for all the relevant model parameters ($\{d_k\}$ and $\{\mathcal{I}^{(m)}\}$). We take as a measure for the quality of a fit the sum of the squares of error,

$$\epsilon(\{d_k\}, \{\mathcal{I}^{(m)}\}) = \sum_j [\mathcal{I}(d(t_j)) - \mathcal{I}_j]^2. \quad (9)$$

Most efficient numerical optimizing algorithms find minima of such an error function by evaluating gradients in parameter space. After obtaining the partial derivatives algebraically, we

may use, for example, the Levenberg–Marquardt algorithm to find the optimal values for all variable parameters (Press *et al.*, 1992). Note that certain parameters may conveniently be excluded from the fitting procedure, if their values are known with sufficient accuracy from other measurements. For example, if the mechanical oscillation frequency Ω and amplitude of the cantilever motion are set externally, one may want to leave these parameters fixed for the fitting process.

Application of the model

As a first test and verification of the fitting procedure, we consider the non-interferometrically detected free oscillation of an aSNOM tip in air. Figure 1 displays typical nominal results for oscillation amplitudes of 80, 159 and 314 nm. The given amplitude values are directly read from the software of the AFM used, and can differ from the real amplitude. The difference will just introduce a scaling $\mathcal{I}'(d) = \mathcal{I}(d/a)$ and would not affect the quality of the fit or otherwise the following discussion. It does point to the need for some additional information (a relationship between the deflection signal and the amplitude, for example) to correctly scale $\mathcal{I}(d)$ with the fitting procedure described here. A possible scheme for aSNOM has recently been discussed by Gucciardi *et al.* (2005).

When fitting our model function to the data, we find first of all that the overall level of residual error is lower for higher amplitudes. This can be attributed to the better signal-to-noise ratio under these conditions. In addition, we verify also that an increase in the number of parameters used generally improves the fit, leading to lower residual errors. For a certain optimal number of mechanical (N_k) and optical (N_m) degrees of freedom, however, the residual error reaches a plateau and a further increase in the number of free parameters does not improve the fit noticeably. This plateau represents the noise level of the measurement beyond which additional model parameters become meaningless. Thus, our model allows to determine the number of significant optical and/or mechanical orders present in a given measured data time trace. For instance, in Fig. 1(a) it is reached for $N_k + N_m > 2$ and in Fig. 1(c) for $N_k + N_m > 5$.

The open question remains, however, how to balance the distribution of optical and mechanical parameters. Only in cases when the noise plateau is reached already by a purely harmonic model can we conclude that neither mechanical nor optical anharmonicities contribute significantly to the measured data. Already for the small amplitude oscillation of Fig. 1(a), for instance, some anharmonicity is present. To illustrate this point further, Fig. 2 displays two possible optimal fits to the data of Fig. 1(b). In Fig. 2(a) a predominantly mechanical origin of the observed anharmonicities is assumed, whereas in (b) an optical anharmonic influence is assumed. Both fits represent the measured time traces equally well,

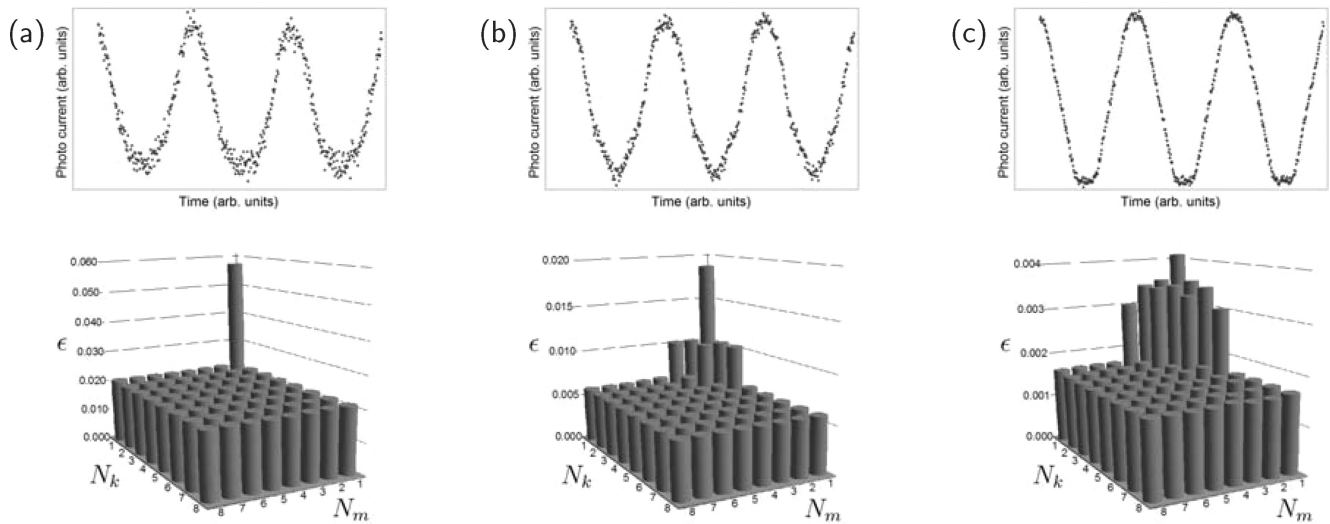


Fig. 1. Upper panels: time traces of the photo current generated by the backscattered radiation collected from the illuminated apex of an aSNOM tip freely oscillating in air. The detection is done non-interferometrically. Lower panels: residual errors ϵ after fitting the nested model expansion $\mathcal{I}(d(t))$ to the measured time series, allowing for different numbers of degrees of freedom in the mechanical (N_k) and optical properties (N_m). The read tip oscillation amplitudes are (a) 80 nm, (b) 159 nm and (c) 314 nm.

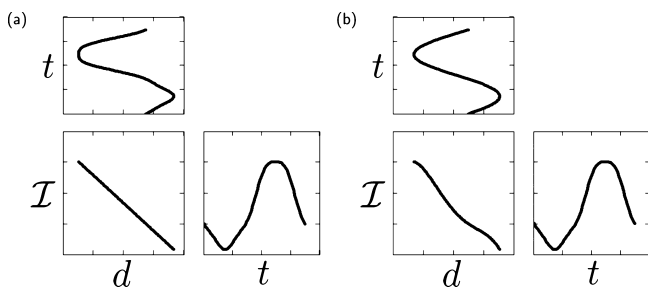


Fig. 2. Two possible fits to the experimental $\mathcal{I}(t)$ trace of Fig. 1(b): (a) assuming mostly mechanical anharmonicity ($N_k = 4, N_m = 1$). (b) assuming mostly optical anharmonicity ($N_k = 1, N_m = 4$). The upper left panels display $d(t)$, the lower left $\mathcal{I}(d)$, and the lower right $\mathcal{I}(t)$, i.e. the fit to the experimental data.

i.e. they are indistinguishable within the noise level. We have to draw the important conclusion that a self-consistent determination of the relative influence of mechanical and optical anharmonicities is not possible within the framework of the present model.

As we are interested in the optical behaviour, a reasonable general approach is to determine the mechanical characteristics of the aSNOM tip oscillation independently, for instance, by recording simultaneously the unfiltered deflection signal used in the AFM distance control feedback. As a first step, this signal would then be analyzed to yield all significant Fourier coefficients d_k entering Eq. (1). Next, these enter as fixed values in a regression analysis of the optical signal time trace with Eq. (9), thus yielding the optical signal versus distance curve $\mathcal{I}(d)$.

Discussion

We have presented a model for the aSNOM signal that is in principle able to reconstruct the optical signal versus tip-sample distance curve. To separate the mechanical from the optical contributions to the signal in practice, the mechanical trace $d(t)$ should be determined independently. If not available, an alternative is to simply ensure harmonic motion as best as possible. Indeed, this is the true and tested path used in many reports on aSNOM measurements.

Where available directly from the experiment (e.g. as the deflection signal of an AFM, if accessible with sufficient bandwidth for accurate determination), the mechanical information can be used as input to the fitting procedure outlined above. In this case the true 3D optical information can be reconstructed even for anharmonic mechanical motion of the probe. This will facilitate decoupling mechanical artefacts (Bek *et al.*, 2005; Billot *et al.*, 2006), which could allow faster scans and the use of bigger drive for the same free space amplitude (Hillenbrand, 2001; Bek *et al.*, 2005)– the latter opening the possibility of stronger near-field interaction at the lower point of the oscillation (Gerton *et al.*, 2004).

In the version presented here, the model signal is treated without any further reference as to how it is related to the actual electromagnetic fields and optical interactions that are being observed. We focus on the electric photocurrent \mathcal{I} generated in the detection process because different varieties of aSNOM setups may translate the optical into electric information quite differently. Linear opto-electronic detectors, for example, may record $\mathcal{I} \propto |\mathbf{E}_s|^2$ in direct non-interferometric or $\mathcal{I} \propto \mathbf{E}_s \cdot \overline{\mathbf{E}_r}$ in homodyne and $\mathbf{E}_s \cdot \overline{\mathbf{E}_r} \exp(i\Omega_r t)$ in heterodyne interferometric detection mode.

(Here, E_s is the scattered electric far field *at the detector* and E_r is a suitable reference field.) Other detection modes are also possible. In all cases, extracting the dependence $E_s(d)$ of the scattered far field on tip-sample distance requires a specifically constructed detection model. Also, an additional model is required for the near-to-far-field transition to facilitate conclusions about the near-field optical interactions at the sample (Esteban *et al.*, 2007).

Any given detection system, though, shares certain general features with the present analysis: Depending on the noise in the measurement, the significant number of orders is found when the residual error cannot be reduced further by including higher order contributions. A self-consistent separation of mechanical and optical influences on the signal is not possible, unless independent input is available such as the deflection signal of the AFM, which determines the mechanical contributions.

Finally we note that the present analysis is applicable beyond the near-field optical microscopic context. *Any* current or voltage signal $I(d)$ or $V(d)$ can be modelled, which depends sensitively on the tip-sample distance. This includes, for instance, thermo-electric effects, capacitive scanning signals, Hall- and Kelvin-probes and others. For any of these effects, our model provides a convenient framework for analysis and extraction of relevant parameters.

References

- Ash, E.A. & Nicholls, G. (1972) Super-resolution aperture scanning microscope. *Nature* **237**, 510–512.
- Barchiesi, D. & Grosjes, T. (2005) Signal reconstruction from a scanning near-field optical microscopy approach curve. *Optics Express* **13**, 6519–6526.
- Bek, A., Vogelgesang, R. & Kern, K. (2005) Optical nonlinearity versus mechanical anharmonicity contrast in dynamic mode apertureless scanning nearfield optical microscopy. *Appl. Phys. Lett.* **87**, 163115-1–163115-3.
- Betzig, E., Trautmann, J.K., Harris, T.D., Weiner, J.S. & Kostelak, R.L. (1991) Breaking the diffraction barrier: optical microscopy on a nanometric scale. *Science* **251**, 1468–1470.
- Billot, L., Lamy de la Chapelle, M., Barchiesi, D., Chang, S.-H., Gray, S.K., Rogers, J.A., Bouhelier, A., Adam, P.-M., Bijeon, J.-L., Wiederrecht, G.P., Bachelot, R. & Royer, P. (2006) Error signal artifact in apertureless scanning near-field optical microscopy. *Appl. Phys. Lett.* **89**, 023105-1–023105-3.
- Diziain, S., Barchiesi, D., Grosjes, T. & Adam, P.-M. (2006) Recovering of the apertureless scanning near-field optical microscopy signal through a lock-in detection. *Appl. Phys. B* **84**, 233–238.
- Esteban, R., Vogelgesang, R. & Kern, K. (2007) Tip-substrate interaction in optical near-field microscopy. *Phys. Rev. B* **75**, 195410-1–195410-8.
- Garcia, R. & Perez, R. (2002) Dynamic atomic force microscopy methods. *Sur. Sci. Rep.* **47**, 197–301.
- Gerton, J.M., Wade, L.A., Lessard, G.A., Ma, Z. & Quake, S.R. (2004) Tip-enhanced fluorescence microscopy at 10 nanometer resolution. *Phys. Rev. Lett.* **93**, 180801-1–180801-4.
- Gucciardi, P.G., Bachelier, G., Mlayah, A. & Allegrini, M. (2005) Interferometric measurement of the tip oscillation amplitude in apertureless-near-field optical microscopy. *Rev. Sci. Instrum.* **76**, 036105-1–036105-3.
- Hartschuh, A., Sanchez, E.J., Xie, X.S. & Novotny, L. (2003) High-resolution near-field raman microscopy of single-walled carbon nanotubes. *Phys. Rev. Lett.* **90**, 095503-1–095503-4.
- Hillenbrand, R. (2001) *Nahfeldoptischeamplituden und Phasenkontrastmikroskopie Zur Nanoskopischen Optischen Abbildung Von Materialkontrast und Optisch Resonanten Partikeln*, Shaker-Verlag, Aachen.
- Hillenbrand, R. & Keilmann, F. (2000) Complex optical constants on a subwavelength scale. *Phys. Rev. Lett.* **85**, 3029–3032.
- Hillenbrand, R., Stark, M. & Guckenberger, R. (2000) Higher-harmonics generation in tapping-mode atomic-force microscopy: insights into the tip-sample interaction. *App. Phys. Lett.* **76**, 3478–3480.
- Hu, D., Micic, M., Klymyshyn, N., Suh, Y.D. & Lu, H.P. (2003) Correlated topographic and spectroscopic imaging beyond diffraction limit by atomic force microscopy metallic tip-enhanced near-field fluorescence lifetime microscopy. *Rev. Sci. Instrum.* **74**, 3347–3355.
- Huang, F.M., Festy, F. & Richards, D. (2005) Tip-enhanced fluorescence imaging of quantum dots. *App. Phys. Lett.* **87**, 183101-1–183101-3.
- Knoll, B. & Keilmann, F. (1999) Near-field probing of vibrational absorption for chemical microscopy. *Nature* **399**, 134–137.
- Knoll, B. & Keilmann, F. (2000) Enhanced dielectric contrast in scattering-type scanning near-field optical microscopy. *Opt. Commun.* **182**, 321–328.
- Lee, S.I., Howell, S.W., Raman, A. & Reifenberger, R. (2002) Nonlinear dynamics of microcantilevers in tapping mode atomic force microscopy: a comparison between theory and experiment. *Phys. Rev. B* **66**, 115409-1–115409-10.
- Lee, S.I., Howell, S.W., Raman, A. & Reifenberger, R. (2003) Nonlinear dynamic perspectives on dynamic force microscopy. *Ultramicroscopy* **97**, 185–198.
- Lewis, A., Isaacson, M., Harootunian, A. & Muray, A. (1984) Development of a 500 Å spatial resolution light microscope. *Ultramicroscopy* **13**, 227–232.
- Martin, Y., Zenhausern, F. & Wickramasinghe, H.K. (1996) Scattering spectroscopy of molecules at nanometer resolution. *Appl. Phys. Lett.* **68**, 2475–2477.
- Ocelic, N. & Hillenbrand, R. (2004) Subwavelength-scale tailoring of surface phonon polaritons by focused ion-beam implantation. *Nat. Mat.* **3**, 606–609.
- Okeefe, J.A. (1956) Resolving power of visible light. *J. Opt. Soc. Am.* **46**, 359–359.
- Pohl, D.W., Denk, W. & Lanz, M. (1984) Optical stethoscopy: image recording with resolution $\lambda/20$. *Appl. Phys. Lett.* **44**, 651–653.
- Press, W.H., Flannery, B., Teukolsky, S.A. & Vetterling, W.T. (1992) *Numerical Recipes in C: The Art of Scientific Computing*, Cambridge University Press, Cambridge, New York.
- Rodriguez, T.R. & Garcia, R. (2004) Compositional mapping of surfaces in atomic force microscopy by excitation of the second normal mode of the microcantilever. *App. Phys. Lett.* **84**, 449–451.
- Stark, M., Stark, R.W., Heckl, W.M. & Guckenberger, R. (2000) Spectroscopy of the anharmonic cantilever oscillations in tapping-mode atomic-force microscopy. *App. Phys. Lett.* **77**, 3293–3295.

- Stark, R.W. (2004) Spectroscopy of higher harmonics in dynamic atomic force microscopy. *Nanotechnology* **15**, 347–351.
- Stark, R.W. & Heckl, W.M. (2003) Higher harmonics imaging in tapping-mode atomic-force microscopy. *Rev. Sci. Instrum.* **74**, 5111–5114.
- Synge, E.H. (1928) A suggested method for extending microscopic resolution into the ultra-microscopic region. *Philos. Mag.* **6**, 356–362.
- Zenhausern, F., Martin, Y. & Wickramasinghe, H.K. (1995) Scanning interferometric apertureless microscopy: Optical imaging at 10 angstrom resolution. *Science* **269**, 1083–1085.
- Zenhausern, F., Oboyle, M.P. & Wickramasinghe, H.K. (1994) Apertureless near-field optical microscope. *Appl. Phys. Lett.* **65**, 1623–1625.